INORGANIC CHEMISTRY
FRONTIERS

RESEARCH ARTICLE

View Article Online
View Journal | View Issue

Cite this: *Inorg. Chem. Front.*, 2023, **10**, 5016

Charge effect in protein metalation reactions by diruthenium complexes†

Aarón Terán, [a] Giarita Ferraro,[b] Ana E. Sánchez-Peláez, [a] Santiago Herrero *[a] and Antonello Merlino *[b]

The properties of paddlewheel diruthenium compounds significantly depend on the nature of the bridging equatorial ligands. The charge of these complexes is a factor to take into account when studying their interaction with proteins. To compare the reactivity of diruthenium compounds with the model protein hen egg white lysozyme (HEWL), we have prepared the well-known anionic complex $[Ru_2(CO_3)_4]^{3-}$, two new anionic species, $[Ru_2(D\text{-}p\text{-}FPhF)(CO_3)_3]^{2-}$ and $[Ru_2(DAniF)(CO_3)_3]^{2-}$, and their analogues $[Ru_2Cl(D\text{-}p\text{-}FPhF)(O_2CCH_3)_3]$ and $[Ru_2Cl(DAniF)(O_2CCH_3)_3]$ that generate cationic species in solution (D-*p*-FPhF$^-$ = *N*,*N*′-bis(4-fluorophenyl)formamidinate and DAniF$^-$ = *N*,*N*′-bis(4-methoxyphenyl)formamidinate). The interaction of these compounds with HEWL was investigated by UV-vis absorption spectroscopy, circular dichroism, intrinsic fluorescence and X-ray crystallography. The molecular structures of the adducts differ in the number of metal binding sites, in the binding mode and in the type of fragments that are bound to the protein. The charge of the diruthenium complexes in aqueous solutions strongly influences their protein binding properties. High-negative charge complexes are non-covalently bound. However, the replacement of carbonate ligands changes the negative charge of these complexes and favours covalent binding. These results have great implications for further studies in the tailoring of artificial diruthenium-containing metalloenzymes.

Received 26th June 2023,
Accepted 11th July 2023

DOI: 10.1039/d3qi01192e

rsc.li/frontiers-inorganic

Introduction

Diruthenium(II,III) paddlewheel complexes contain a Ru–Ru core bridged by four equatorial ligands, which in the first compounds, synthesized by Wilkinson and Cotton, were carboxylates.[1,2] In the solid state, they can show polymeric structures with axial ligands bridging the diruthenium units to form linear or zig-zag chains, discrete molecular species or cation–anion complexes.[3,4] Besides carboxylates, a variety of *N*,*O*- and *N*,*N*′-bridging bidentate ligands have been employed to obtain diverse diruthenium motifs.[5–9]

The synthesis and reactivity of these complexes have been intensively studied in the last few years due to their singular electrochemical[10,11] and magnetic properties.[12–16] Diruthenium(II,III) paddlewheel complexes have also been used as scaffolds to prepare anticancer agents[17–25] and to produce stable metalloenzymes with fascinating catalytic properties.[26,27] In this frame, it has been shown that $[Ru_2(O_2CCH_3)_4]^+$ forms a metalloenzyme with the model protein hen egg white lysozyme (HEWL)[26] which is able to catalyse the aerobic oxidation of hydroxylamines to nitrones imparting complete chemoselectivity to the reaction, in contrast to the metal complex alone.[27]

In our continuous effort to study the reactivity of metal compounds with physiologically relevant molecules such as proteins, we have recently described the interaction of $[Ru_2(D\text{-}p\text{-}FPhF)(O_2CCH_3)_3]^+$ (D-*p*-FPhF$^-$ = *N*,*N*′-bis(4-fluorophenyl)formamidinate) with HEWL under different conditions in order to compare the effect of bulky equatorial ligands.[28] The introduction of a formamidinate ligand increases the stability of the diruthenium core in solution. It has been shown that under all circumstances the formamidinate ligand is retained. In addition, this *N*,*N*′-bridging ligand can adopt a *cis* or a *trans* configuration with respect to the bridging coordinating residue side chains. The diruthenium core not only can bind at the equatorial positions of the side chain of Asp101 and 119, but also can bind to the Lys or Arg side chains or even the oxygen atom of a main chain carbonyl group at the axial sites.

The diruthenium(II,III) compounds employed until now to study their interaction with proteins form monocationic species in solution. The charge of the diruthenium complexes

[a]*MatMoPol Research Group, Department of Inorganic Chemistry, Faculty of Chemical Sciences, Complutense University of Madrid, Avda. Complutense s/n, 28040 Madrid, Spain. E-mail: sherrero@ucm.es*
[b]*Department of Chemical Sciences, University of Naples Federico II, Complesso Universitario di Monte Sant'Angelo, via Cinthia, 21, 80126 Naples, Italy. E-mail: antonello.merlino@unina.it*

† Electronic supplementary information (ESI) available. See DOI: https://doi.org/10.1039/d3qi01192e

is expected to affect the type of adducts that will be formed upon reaction of the compounds with proteins.[29] In this regard, anionic species may be the door towards a new family of diruthenium metalloproteins. However, the number of known anionic diruthenium complexes is rather limited and most of them contain two labile anionic ligands at the axial positions.[30–34] Another possibility is the use of high-charge anionic bridging ligands. In fact, our group and others have been interested in the use of the anionic unit $[Ru_2(CO_3)_4]^{3-}$ to develop heterometallic building blocks with different topologies and interesting magnetic properties.[35–43]

Here we report the synthesis and characterization of $K_3[Ru_2(CO_3)_4]$, $K_2[Ru_2(DAniF)(CO_3)_3]$, $K_2[Ru_2(D\text{-}p\text{-}FPhF)(CO_3)_3]$, and $[Ru_2Cl(DAniF)(O_2CCH_3)_3]$ ($DAniF^-$ = *N*,*N*′-bis(4-methoxyphenyl)formamidinate; Fig. 1) to prepare new diruthenium metalloproteins. We show crystallographic evidence of different binding modes depending on the cationic/anionic nature of the complexes in aqueous solutions ($[Ru_2(CO_3)_4]^{3-}$, $[Ru_2(D\text{-}p\text{-}FPhF)(CO_3)_3]^{2-}$, $[Ru_2(DAniF)(CO_3)_3]^{2-}$, and $[Ru_2(DAniF)(O_2CCH_3)_3]^{+}$). Data have been compared with those reported for $[Ru_2(O_2CCH_3)_4]^{+}$ and $[Ru_2(D\text{-}p\text{-}FPhF)(O_2CCH_3)_3]^{+}$ complexes.[26,28]

Results and discussion

Synthesis and characterization of $K_2[Ru_2(D\text{-}p\text{-}FPhF)(CO_3)_3]$ and $K_2[Ru_2(DAniF)(CO_3)_3]$

The preparation of $K_3[Ru_2(CO_3)_4]\cdot 4H_2O$ and $[Ru_2Cl(DAniF)(O_2CCH_3)_3]\cdot H_2O$ derivatives is already described in the literature.[44,45] Here, the synthesis of two new heteroleptic anionic complexes, $K_2[Ru_2(D\text{-}p\text{-}FPhF)(CO_3)_3]\cdot 3H_2O\cdot EtOH$ and $K_2[Ru_2(DAniF)(CO_3)_3]\cdot 3H_2O$, from the corresponding $[Ru_2Cl(L\text{–}L)(O_2CCH_3)_3]$ is reported (Scheme S1, ESI†). The replacement of acetate by carbonate bridging ligands proceeds successfully overnight under mild conditions in 95–99% yields. All the diruthenium complexes are air stable and water-soluble and can be handled without special caution. The new complexes were determined by elemental analysis, ATR-FT-IR (attenuated total reflection Fourier transform infrared) spectroscopy, UV-Vis spectroscopy, electrospray ionization mass spectrometry and cyclic voltammetry.

The ATR-FTIR spectra of the compounds (Fig. S1, ESI†) are similar to each other and to their analogs with acetate ligands. A wide band in the 3500–3400 cm^{-1} range and a band centred around 1640 cm^{-1} suggest the presence of water in both complexes, in accordance with elemental analysis. Carbonate vibrational modes corresponding to COO stretching (asymmetric + symmetric) and bending can be observed around 1450 and 694 cm^{-1}, respectively. Some of the formamidinato ligand vibration modes are observed at 1529 cm^{-1} ($\nu(C{=}C_{arom})$) and 1296 and 1210 cm^{-1} ($\nu(C\text{–}N)$).[46] These results confirmed the presence of representative functional groups coordinated to the diruthenium core.

Electrospray ionization mass spectrometry was used to verify the stoichiometry and elemental composition of the diruthenium complexes. The mass spectra of $K_2[Ru_2(D\text{-}p\text{-}FPhF)(CO_3)_3]\cdot 3H_2O\cdot EtOH$ and $K_2[Ru_2(DAniF)(CO_3)_3]\cdot 3H_2O$ support the full exchange of all acetate molecules by carbonate ligands retaining the formamidinate ligand. The dominant peaks correspond to the intact complex with the loss of solvent molecules (S = H_2O and/or EtOH), $[M - S + H^+]^+$, or with the ionized forms by loss of K^+ counterions and solvent molecules, $[M - K^+ - S + 2H^+]^+$ and $[M - 2K^+ - S + 3H^+]^+$. All the ion peaks show reasonable agreement between the experimental and simulated isotopic distribution and support the assigned stoichiometries and formulations of the new diruthenium derivatives (Fig. S2 and S3, respectively, ESI†).

Cyclic voltammetry (CV) was used to evaluate the effect of ligand substitution on the electrochemical responses of diruthenium complexes in aqueous solutions. CV measurements were carried out in 0.10 M KCl solution at 0.1 V s^{-1} (Fig. S4, ESI†); the data were compared with those obtained for $[Ru_2Cl(DAniF)(O_2CCH_3)_3]$[45] (reversible one-electron reduction, $Ru_2^{5+/4+}$) and $[Ru_2Cl(D\text{-}p\text{-}FPhF)(O_2CCH_3)_3]$[47] (quasi-reversible one-electron reduction, $Ru_2^{5+/4+}$). The properties of $[Ru_2Cl(O_2CCH_3)_4]$[9] (quasi-reversible one-electron reduction, $Ru_2^{5+/4+}$) and $K_3[Ru_2(CO_3)_4]$[44] (quasi-reversible one-electron oxidation, $Ru_2^{5+/6+}$) were also measured because they had been previously reported under different conditions. Table 1 presents the half-wave peak potentials ($E_{1/2}$) and anodic to cathodic peak potential separation (ΔE) for $[Ru_2Cl(O_2CCH_3)_4]$, $K_3[Ru_2(CO_3)_4]$, $[Ru_2Cl(L\text{–}L)(O_2CCH_3)_3]$ and $K_2[Ru_2(L\text{–}L)(CO_3)_3]$ (L–L = $DAniF^-$

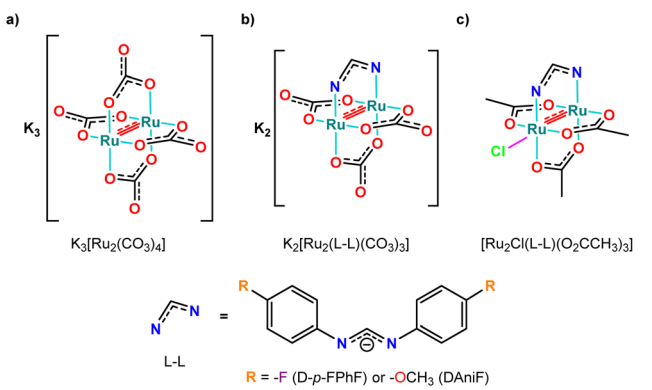

Fig. 1 Molecular structure of diruthenium derivatives: (a) $K_3[Ru_2(CO_3)_4]$, (b) $K_2[Ru_2(DAniF)(CO_3)_3]$ and $K_2[Ru_2(D\text{-}p\text{-}FPhF)(CO_3)_3]$, and (c) $[Ru_2Cl(DAniF)(O_2CCH_3)_3]$ and $[Ru_2Cl(D\text{-}p\text{-}FPhF)(O_2CCH_3)_3]$.

Table 1 Electrochemical data (V *vs.* Ag/AgCl) from cyclic voltammetry measurements of diruthenium complexes in 0.10 M KCl aqueous solutions

Compound	$E_{1/2}$	ΔE
$[Ru_2Cl(O_2CCH_3)_4]$	−0.10	0.27
$K_3[Ru_2(CO_3)_4]$	0.68	0.21
$[Ru_2Cl(D\text{-}p\text{-}FPhF)(O_2CCH_3)_3]$	−0.32	0.28
$K_2[Ru_2(D\text{-}p\text{-}FPhF)(CO_3)_3]$	0.75	0.08
$[Ru_2Cl(DAniF)(O_2CCH_3)_3]$	−0.35	0.15
$K_2[Ru_2(DAniF)(CO_3)_3]$	0.68	0.08

or D-*p*-FPhF$^-$) derivatives. Formamidinate[10] (L–L) and carbonate[44] ligands increase the electron density on the diruthenium core and seem to favour a $Ru_2^{5+/6+}$ reversible oxidation process. Besides, the presence of electron-donating substituents in the aromatic rings (–OCH_3) produces lower oxidation potentials, while the presence of an electron-withdrawing substituent (–F) causes a positive cathodic shift.

Stability of $[Ru_2(CO_3)_4]^{3-}$, $[Ru_2(D\text{-}p\text{-}FPhF)(CO_3)_3]^{2-}$, $[Ru_2(DAniF)(CO_3)_3]^{2-}$ and $[Ru_2(DAniF)(O_2CCH_3)_3]^+$ in aqueous solutions

To ascertain the stability of $[Ru_2(CO_3)_4]^{3-}$, $[Ru_2(D\text{-}p\text{-}FPhF)(CO_3)_3]^{2-}$, $[Ru_2(DAniF)(CO_3)_3]^{2-}$ and $[Ru_2(DAniF)(O_2CCH_3)_3]^+$ in aqueous solutions and under the conditions used to study their binding to HEWL, UV-Vis absorption spectra were collected as a function of time.

The monitoring of the UV-Vis bands of the four compounds in pure water and in different buffers is reported (Fig. S5 and S6–S9 panels A and C, ESI†). In the visible region (400–700 nm), absorptions bands are assigned to allowed ligand-to-metal charge transfers [π(N/O), π(axial) → $\pi^*(Ru_2)$], while the UV bands are usually related to an axial ligand-to-metal charge transfer and ligand-to-metal transitions [π(N) → $\sigma^*/\pi^*/\delta^*(Ru_2)$].[9,28] No appreciable spectral changes were observed within 24 h. However, under the conditions used for the crystallization experiments, some changes were found after a week. In all cases, the absorption profiles show regularity in the shape and position of the bands and are very similar to other monosubstituted diruthenium compounds. Slight variations due to a possible substitution of the *O*,*O*′-donor equatorial ligands (acetates or carbonates) for other *O*,*O*′-donor ligands present under the corresponding conditions (*e.g.*, nitrates, acetates, or formates) are noticed. This is related to the high concentration of these ions in the buffer medium which may lead to different partial substitution reactions.[48] Spectra were also collected as a function of time in the presence of HEWL under the same experimental conditions. Under almost all of the conditions used for the crystallization experiments, no significant differences between the spectral profiles of the compounds in the absence and in the presence of the protein are evidenced (Fig. S6–S9 panels B and D, ESI†).

Binding to HEWL: fluorescence and circular dichroism studies

To further study the HEWL binding ability of $[Ru_2(CO_3)_4]^{3-}$, $[Ru_2(D\text{-}p\text{-}FPhF)(CO_3)_3]^{2-}$, $[Ru_2(DAniF)(CO_3)_3]^{2-}$ and $[Ru_2(DAniF)(O_2CCH_3)_3]^+$, intrinsic fluorescence and circular dichroism (CD) measurements were collected. First, the fluorescence quenching measurements were registered (Fig. 2A–D and Fig. S10–S13, ESI†). Basically, HEWL fluorescence is caused by tryptophan, tyrosine and phenylalanine residues (n → π^* transition). As a result of the binding, an enhancement or a decrease of the fluorescence should occur. Titration experiments carried out by adding $[Ru_2(CO_3)_4]^{3-}$, $[Ru_2(D\text{-}p\text{-}FPhF)(CO_3)_3]^{2-}$, $[Ru_2(DAniF)(CO_3)_3]^{2-}$ and $[Ru_2(DAniF)(O_2CCH_3)_3]^+$ to a HEWL solution show a reduction of the fluorescence intensity of the protein, thus indicating that all these metal compounds could bind to the protein under the investigated experimental conditions.

Circular dichroism (CD) spectroscopy provides information on the protein secondary structure content and can be used to investigate the structure and dynamics of interactions of proteins with foreign moieties. Far-UV CD spectra of HEWL at 25 °C in the absence and in the presence of the four compounds at different HEWL : Ru_2 molar ratios in 10 mM Hepes buffer pH 7.5 and 10 mM sodium acetate buffer pH 4.0 were collected and are reported in Fig. 2E–H and Fig. S14, ESI,† respectively. The spectrum of metal-free HEWL presents a double minimum at 208 and 222 nm, as expected for a protein with a large content of α-helix structural elements. Surprisingly, we noticed that the addition of some Ru_2^{5+} compounds caused an increase in the negative ellipticity without any significant shift of the bands. Previous results with the $[Ru_2(D\text{-}p\text{-}FPhF)(O_2CCH_3)_3]^+$ complex[28] showed that the incubation of this compound with the protein did not change the CD spectrum. In this case, its anionic analogue, $[Ru_2(D\text{-}p\text{-}FPhF)(CO_3)_3]^{2-}$, did not significantly change the CD signal. However, with compounds $[Ru_2(CO_3)_4]^{3-}$, $[Ru_2(DAniF)(CO_3)_3]^{2-}$ and $[Ru_2(DAniF)(O_2CCH_3)_3]^+$, an increase in the negative ellipticity signal is observed. This can be associated with a kosmotropic-like property of these diruthenium derivatives. A kosmotrope strengthens the hydrogen bonds of water molecules and stabilizes the intramolecular interactions in the structure of a biomolecule.[49] The increase of self-association processes within the HEWL chain, in the presence of diruthenium complexes, can create a more prevalent secondary structure which would increase the CD signal.[50,51] In all cases, the global stabilization of the protein secondary structure produced upon interaction with the diruthenium species is not associated with a change in their thermal denaturation, since the protein in the presence of the diruthenium complexes has almost the same denaturation temperature as in their absence (Table S1, ESI†). The character of the changes suggests that the diruthenium-induced variations do not generate a different conformation but more likely affect the compactness/dynamics of the polypeptide chain. This phenomenon seems to be quite significant, especially for the DAniF derivatives, where the presence of the methoxy group is expected to generate a higher number of interactions with the surrounding water molecules.

Binding to HEWL: crystallographic studies

X-ray crystallography was used to study the structure of the adducts formed upon the reaction of HEWL with $[Ru_2(CO_3)_4]^{3-}$, $[Ru_2(D\text{-}p\text{-}FPhF)(CO_3)_3]^{2-}$, $[Ru_2(DAniF)(CO_3)_3]^{2-}$, and $[Ru_2(DAniF)(O_2CCH_3)_3]^+$. The structures of the adducts were prepared by a soaking method using protein crystals grown under two different experimental conditions: 20% ethylene glycol, 0.6 M sodium nitrate, and 0.1 M sodium acetate pH 4.0 (**condition A**) and 2 M sodium formate and 0.1 M Hepes (*N*-2-hydroxyethylpiperazine-*N*′-2-ethanesulfonic acid), pH 7.5 (**condition B**). The crystals of the adducts were freezed after 14 days of soaking. They diffracted X-ray at a resolution within the range of 1.46–1.03 Å. Data collection and refinement statistics

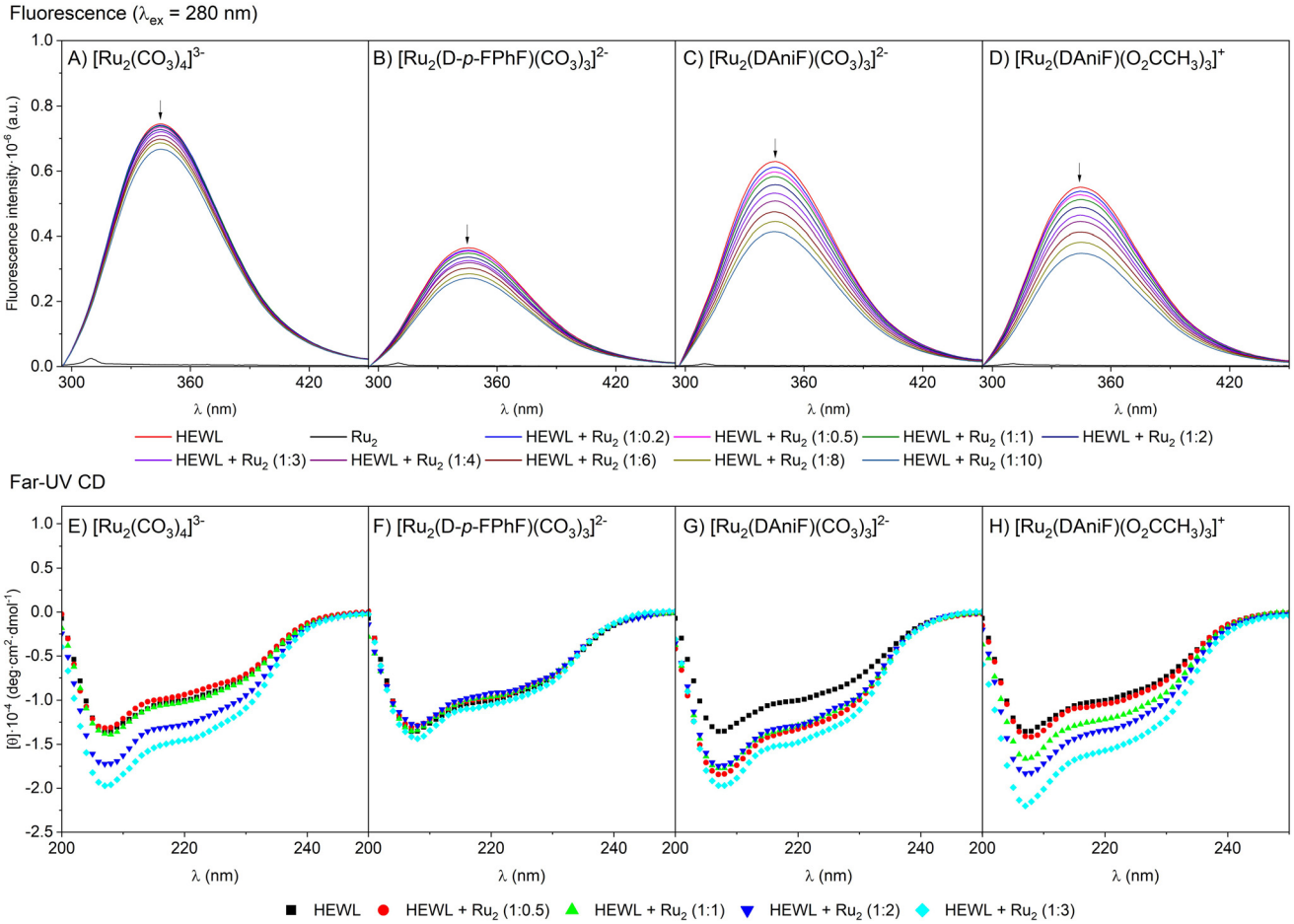

Fig. 2 (A–D) Fluorescence quenching spectra of HEWL (2 μM) in 10 mM Hepes buffer pH 7.5 by $[Ru_2(CO_3)_4]^{3-}$ (A), $[Ru_2(D\text{-}p\text{-}FPhF)(CO_3)_3]^{2-}$ (B), $[Ru_2(DAniF)(CO_3)_3]^{2-}$ (C), and $[Ru_2(DAniF)(O_2CCH_3)_3]^{+}$ (D) (upon increasing the concentrations from 0 to 20 μM). Spectra exciting the protein at 295 nm are reported in the ESI.† At the concentration used for these experiments the metal compounds do not significantly absorb. (E–H) Far-UV CD spectra of HEWL (7.0 μM concentration) incubated for 24 h in the presence of $[Ru_2(CO_3)_4]^{3-}$ (E), $[Ru_2(D\text{-}p\text{-}FPhF)(CO_3)_3]^{2-}$(F), $[Ru_2(DAniF)(CO_3)_3]^{2-}$ (G), and $[Ru_2(DAniF)(O_2CCH_3)_3]^{+}$ (H) in 10 mM Hepes buffer pH 7.5 in different HEWL : Ru_2 molar ratios.

are reported in Table S2, ESI.† The structures refine to R_{factor} and R_{free} values within the range of 0.179–0.205 and 0.202–0.245, respectively. Analysis of the Fourier difference electron density map indicated that attempts to obtain crystals of the adduct of $[Ru_2(CO_3)_4]^{3-}$ with HEWL under **condition B** failed. The structures are deposited in the PDB (**https://www.rcsb.org**) as entries 8PFU (HEWL with $[Ru_2(CO_3)_4]^{3-}$ under **condition A**), 8PFT (HEWL with $[Ru_2(D\text{-}p\text{-}FPhF)(CO_3)_3]^{3-}$ under **condition A**), 8PFX (HEWL with $[Ru_2(D\text{-}p\text{-}FPhF)(CO_3)_3]^{3-}$ under **condition B**), 8PFW (HEWL with $[Ru_2(DAniF)(CO_3)_3]^{2-}$ under **condition A**), 8PFY (HEWL with $[Ru_2(DAniF)(CO_3)_3]^{2-}$ under **condition B**) and 8PFV (HEWL with $[Ru_2(DAniF)(O_2CCH_3)_3]^{+}$ under **condition A**).

Structure of the adduct formed upon the reaction of HEWL with $[Ru_2(CO_3)_4]^{3-}$ under condition A

The overall structure of the adduct that HEWL forms with $[Ru_2(CO_3)_4]^{3-}$ under **condition A** (Fig. 3), which was refined at a resolution of 1.18 Å, is nearly identical to that of the metal-

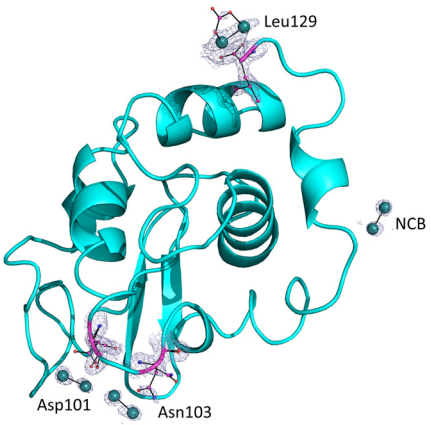

Fig. 3 Diruthenium binding sites in the structure of the adduct formed upon the reaction of HEWL with $[Ru_2(CO_3)_4]^{3-}$ after 14 days of soaking under **condition A**. $2F_o - F_c$ electron density maps are contoured at the 1.0σ (grey) level.

free protein: the root mean square deviation of the carbon alpha atoms (rmsd) between the structure of the adduct and that of the HEWL used as a starting model (PDB code: 193L[52]) is as low as 0.12 Å. The main differences are located at the level of the diruthenium binding sites. In the structure of the adduct, diruthenium centres are found close to the interface between two symmetry-related molecules (occupancy = 0.20) and at the side chains of Asn103 (occupancy = 0.2 and the distance from the nearest protein atom ≈ 2.1 Å) and Asp101 (occupancy = 0.20 and the distance Ru-OD ≈ 2.5 Å). In all these sites, diruthenium ligands cannot be defined. *B*-factors of Ru atoms are within the range of 63.6–28.6 Å^2. Our data suggest that under the investigated experimental conditions, diruthenium tetracarbonate loses at least a part of the carbonate ligands and that a diruthenium containing fragment, probably coordinated to solvent molecules and to a part of carbonate ligands originally present in the $[Ru_2(CO_3)_4]^{3-}$ structure, can react with the protein. An additional diruthenium centre was found at the C-terminal tail (distance Ru-OX ≈ 2.2 Å), non-covalently bound to the protein. Here the ligands are not well defined, but one carbonate could be bound to the metals. At this site, Ru atoms have an occupancy of 0.40 and *B*-factors of 63.6 and 42.8 Å^2.

Structures of the adducts formed upon the reaction of HEWL with the $[Ru_2(D\text{-}p\text{-}FPhF)(CO_3)_3]^{2-}$ complex

Superimposition of the structures of the adducts formed upon the reaction of HEWL with $[Ru_2(D\text{-}p\text{-}FPhF)(CO_3)_3]^{2-}$ under **conditions A** and **B** gave a rmsd value of 0.15 Å, suggesting similarity of the overall protein conformation in the adducts obtained under the two conditions (Fig. 4A and 5A). Similar results were obtained upon superimposition of these structures with that of the metal-free protein (rmsd = 0.16 Å for **conditions A** and **B**). The structure obtained under **condition A** was resolved at 1.30 Å resolution, while that under **condition B** was resolved at 1.03 Å resolution.

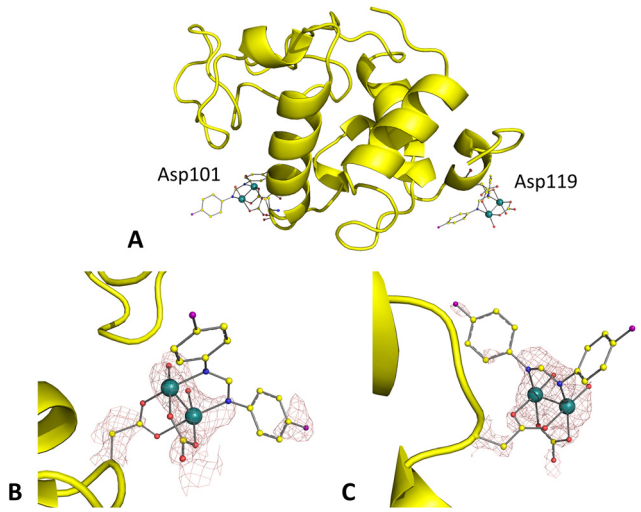

Fig. 4 Diruthenium binding sites in the structure of the adduct formed upon the reaction of HEWL with $[Ru_2(D\text{-}p\text{-}FPhF)(CO_3)_3]^{2-}$ after 14 days of soaking under **condition A** (panel A). Binding sites have been observed close to the side chains of Asp101 (panel B) and Asp119 (panel C). $2F_o - F_c$ electron density maps are contoured at the 1.0 σ (grey) level.

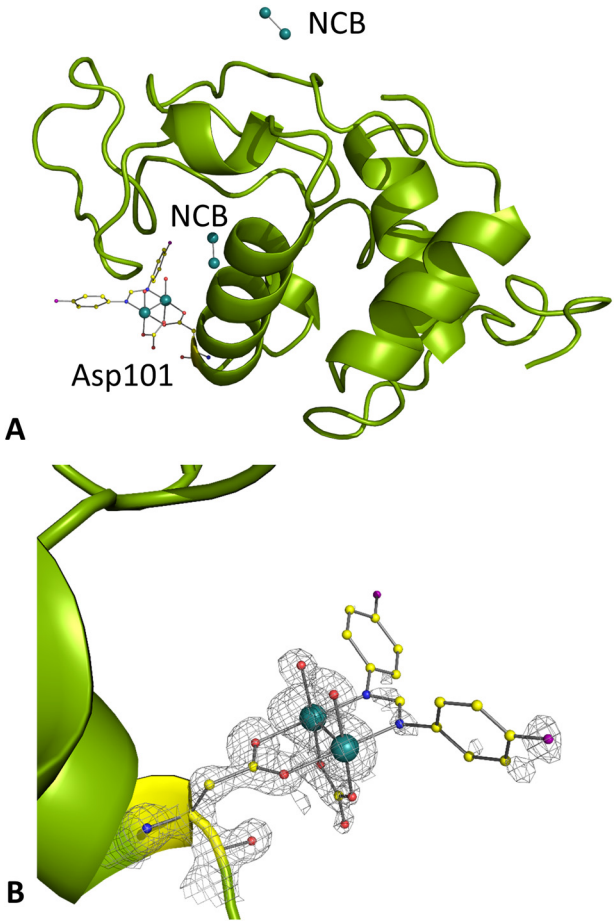

Fig. 5 Covalent and non-covalent (NCB) diruthenium binding sites in the structure of the adduct formed upon the reaction of HEWL with $[Ru_2(D\text{-}p\text{-}FPhF)(CO_3)_3]^{2-}$ after 14 days of soaking under **condition B** (panel A). Binding sites have been observed close to the side chain of Asp101 (panel B). $2F_o - F_c$ electron density maps are contoured at the 1.0 σ (grey) level. Axial H_2O molecules are omitted for the sake of clarity.

In the crystal structure of the adduct formed upon the reaction of HEWL with $[Ru_2(D\text{-}p\text{-}FPhF)(CO_3)_3]^{2-}$ under **condition A** (Fig. 4A), resolved at 1.42 Å resolution, electron density for two diruthenium containing fragments (occupancy = 0.35) was observed (Fig. 4B and C). The side chain of Asp101 is coordinated to the diruthenium core together with D-*p*-FPhF, a carbonate ion, and two equatorial and two axial water molecules, $[Ru_2(Asp101)(D\text{-}p\text{-}FPhF)(CO_3)(OH_2)_4]^+$ (Fig. 4B). D-*p*-FPhF is *trans* to the side chain of the Asp (Fig. 4B). In our model this diruthenium center was interpreted as an alternative to that found close to Asp119. The second diruthenium fragment is the same found close to Asp101, *i.e.*, a $[Ru_2(Asp119)(D\text{-}p\text{-}FPhF)(CO_3)(OH_2)_4]^+$ moiety. This fragment has the D-*p*-FPhF *cis* to the side chain of Asp119 (Fig. 4C). These findings confirm that anionic monosubstituted diruthenium paddlewheel complexes can bind to protein residue side chains both in *cis* and *trans*

configurations as their cationic analogs.[28] In any case, since the occupancy is low, the coordination of an anion bridging ligand instead of two water molecules cannot be excluded (Fig. 4B).

Under **condition B**, crystals of the adduct diffract at 1.03 Å resolution. Here, diruthenium containing fragments were observed close to the side chain of Asp101 (Fig. 5A) and close to a symmetry axis (Fig. 5B). A Hepes molecule was also added to the model (Fig. S15†). A $[Ru_2(Asp101)(D\text{-}p\text{-}FPhF)(CO_3)(OH_2)_4]^+$ moiety was formed similarly to that obtained under **condition A**. At this site, the diruthenium fragment presents an occupancy equal to 0.35. The *B*-factors of Ru atoms are 15.4 and 14.4 Å^2. Two water molecules complete the octahedral coordination sphere of each Ru atom occupying the axial sites. An extra electron density neighbouring this diruthenium fragment was observed in the $F_o - F_c$ and in the anomalous difference electron-density maps. Here two Ru atoms were placed in the model, not coordinated to any residue side chains and with low occupancy (0.20) and *B*-factors of 15.5 and 14.5 Å^2. Diruthenium centre ligands at this site are undefined. Another disordered Ru_2-containing fragment, non-covalently bound to HEWL and with occupancy 0.20 (*B*-factors of 16.1 and 17.9 Å^2), was found close to the symmetry axis. Here the ligands are not well defined.

Structures of the adducts formed upon the reaction of HEWL with the $[Ru_2(DAniF)(CO_3)_3]^{2-}$ complex

Crystals of the HEWL adducts with $[Ru_2(DAniF)(CO_3)_3]^{2-}$ obtained upon soaking of the metal compound within HEWL crystals grown under **conditions A** and **B** were also analysed. The structure of the adduct obtained under **condition B** (at a resolution of 1.19 Å) suggests a scarce binding of the compound to the protein. Only one minor peak of anomalous difference electron density map is observed in this structure, close to the Asp101 side chain (data not shown). In contrast, very clear electron density maps are observed in the structure of the adduct formed under **condition A** (at a resolution of 1.12 Å). Here, three different metal compound binding sites were found (Fig. 6A).

The first diruthenium centre (occupancy = 0.50) is linked to the side chain of Asp119 *cis* to the DAniF ligand together with two equatorial carbonate ligands and two axial water molecules, $[Ru_2(Asp119)(DAniF)(CO_3)_2(OH_2)_2]^-$ (Fig. 6C). The other two binding sites are found on the protein surface, where the diruthenium complexes are non-covalently bound to the protein (Fig. 6B and C). In both cases, the whole compound is modeled: a diruthenium compound that retains all its carbonate and DAniF ligands at the equatorial positions and with water molecules at the axial sites, $[Ru_2(DAniF)(CO_3)_3(OH_2)_2]^{2-}$. The presence of carbonate ligands coordinated to the diruthenium center and a methoxy group attached to the aromatic rings of the formamidinate ligand (DAniF) allows one to establish different interactions which stabilize the Ru_2/HEWL adduct. One molecule (occupancy = 0.35) is close to Asp101 (Fig. 6D) and interacts with a NO_3^- ion and with the side chains of Ser100, Lys97 and Gly102. Also, interactions with

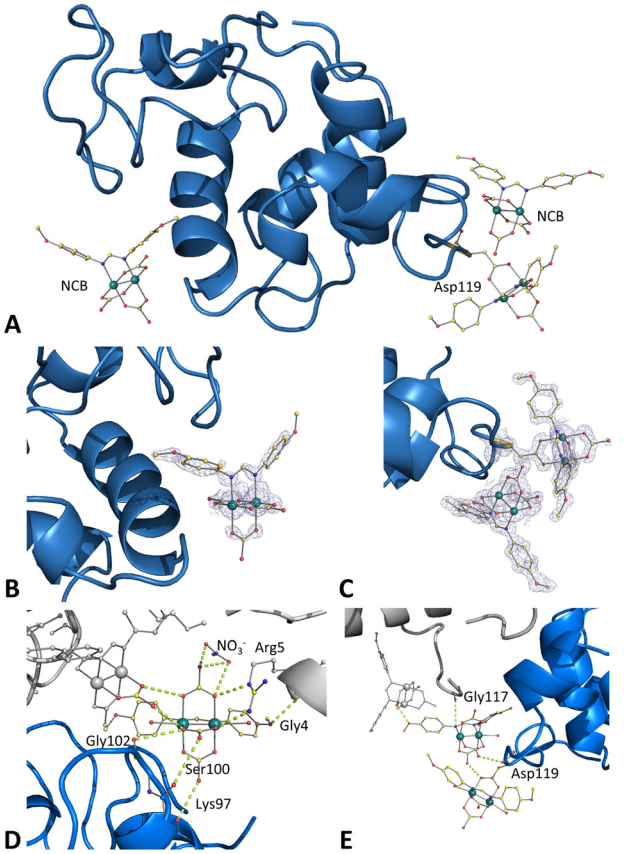

Fig. 6 Overall structure of the adduct formed upon the reaction of HEWL with $[Ru_2(DAniF)(CO_3)_3]^{2-}$ under **condition A** (panel A) and details of the diruthenium covalent and non-covalent binding (NCB) sites (panels B–E). $2F_o - F_c$ electron density maps are contoured at the 1.0 σ (grey) level. Symmetry related molecules are colored grey. Axial H_2O molecules are omitted for the sake of clarity.

symmetry mates occur through the side chains of Arg5 and Gly4 and with the carbonate group of other diruthenium motif coordinated to Asp119. The second Ru_2 complex (occupancy = 0.45) is close to Asp119 (Fig. 6E) and interacts with the main chain carbonyl group of Asp119 and with the carbonate group of the diruthenium complex bound to the side chain of Asp119. Here, the carbonate ligands interact with a symmetry-related molecule at the side chain of Gly117 and with the carbonate group of a non-covalently bound diruthenium complex. The *B*-factors of Ru atoms in this structure are within the range of 12.8–9.9 Å^2.

Structures of the adducts formed upon the reaction of HEWL with the $[Ru_2(DAniF)(O_2CCH_3)_3]^+$ complex

To compare the results obtained with $[Ru_2(DAniF)(CO_3)_3]^{2-}$ with a proper reference, the X-ray structure of the adducts of HEWL with $[Ru_2(DAniF)(O_2CCH_3)_3]^+$ formed under **condition A** was also resolved (Fig. 7A).

The structure, which refines at 1.46 Å resolution, reveals the existence of a single binding site for $[Ru_2(DAniF)(O_2CCH_3)_3]^+$, close to the side chain of Asp119 (occupancy = 0.35), with the

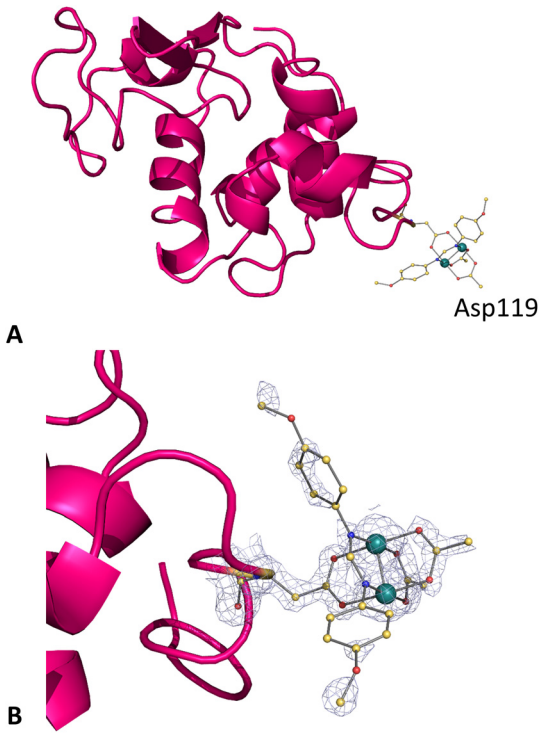

Fig. 7 Overall structure of the adduct formed upon the reaction of HEWL with $[Ru_2(DAniF)(O_2CCH_3)_3]^+$ under **condition A** (panel A) and details of the metal compound binding sites (panel B). $2F_o - F_c$ electron density maps are contoured at the 1.0 σ (grey) level. Axial H_2O molecules are omitted for the sake of clarity.

diruthenium centre bound to the side chain of the Asp residue *cis* to the DAniF ligand (Fig. 7B). Thus, in both the adducts of HEWL with $[Ru_2(DAniF)(CO_3)_3]^{2-}$ and $[Ru_2(DAniF)(O_2CCH_3)_3]^+$ binding to the Asp119 side chain, with the Asp bound *cis* to the formamidinate ligand, occurs. Thus, non-covalent binding was identified in the adduct of the protein with the anionic compound, while only the coordinative mode of binding was observed for $[Ru_2(DAniF)(O_2CCH_3)_3]^+$.

Structural comparison

The structures of the adducts of two paddlewheel diruthenium compounds formed upon the reaction with HEWL have been resolved up to now, $[Ru_2(O_2CCH_3)_4]^+$ and $[Ru_2(D\text{-}p\text{-}FPhF)(O_2CCH_3)_3]^+$.[26,28] These data represent the only structural information on protein adducts of diruthenium compounds. $[Ru_2(O_2CCH_3)_4]^+$ binds to the side chains of Asp residues, losing one acetate ligand in favour of the Asp carboxylate and with the possibility to lose other acetate ligands in favour of water molecules. Upon reaction of the same protein with $[Ru_2(D\text{-}p\text{-}FPhF)(O_2CCH_3)_3]^+$, diruthenium centres are bound to solvent-exposed protein residue side chains (Asp101, Asp119, Asn19, Lys33, and Arg125), retaining the formamidinate ligand, and with different reactivity depending on the experimental conditions.

Comparing the behaviour of $[Ru_2(CO_3)_4]^{3-}$ and $[Ru_2(O_2CCH_3)_4]^+$, it emerges that the different charge of the two complexes does produce significant differences in the reactivity with HEWL: both complexes bind to the Asp side chains, but the tetracarbonate compound can also bind to the Asn side chain and the C-terminal tail and can bind to the protein in a non-covalent fashion. In the case of $[Ru_2(D\text{-}p\text{-}FPhF)(CO_3)_3]^{2-}$ and $[Ru_2(DAniF)(CO_3)_3]^{2-}$, two types of Ru_2 fragments are described: those coordinated to Asp101 or Asp119 side chains and those that are non-covalently bound to the protein surface. The binding Asp residues are shared with their cationic analogues. However, there is a clear influence of the charge on the diruthenium compound binding to the protein, because as long as the complexes retain their high-negative charge (−2) they remain non-covalently bound to the protein. When the loss (or the replacement) of carbonate ligands occurs, *i.e.*, when the complexes reduce their charge from −2 to −1 or they change from an anionic to a cationic form, they directly coordinate with the protein residue side chains, similarly to the cationic diruthenium compounds containing acetate ligands. Once the usual binding sites are occupied, additional molecules will remain on the surface interacting through charge or dipole interactions with adjacent groups, allowing stabilisation of the adduct structure. Thus, the non-covalent binding may be a step that precedes the coordination of the covalently bounded species to the protein, but it also can be the consequence of the full occupancy of the metal binding sites and of the charge of the compound. Notably, our data suggest that it is in principle possible to guide the diruthenium compound protein binding from non-covalent to covalent by substitution of carbonate ions by other ligands.

Conclusions

Structural studies on the products of the reaction of peptides and proteins with diruthenium paddlewheel complexes are important since they provide the molecular basis to explain the behaviour of artificial diruthenium-containing enzymes. These studies are also useful to define the interaction occurring *in vivo* when diruthenium paddlewheel complexes are used as metallodrugs. Here, we have reported six new crystal structures of the adducts formed upon the reaction of HEWL with four distinct diruthenium complexes: $[Ru_2(CO_3)_4]^{3-}$, $[Ru_2(D\text{-}p\text{-}FPhF)(CO_3)_3]^{2-}$ $[Ru_2(DAniF)(CO_3)_3]^{2-}$, and $[Ru_2(DAniF)(O_2CCH_3)_3]^+$.

Cationic diruthenium species react with HEWL by coordinating the side chains of Asp119 and Asp101 upon releasing one or two acetate ligands. In contrast, anionic diruthenium complexes may be non-covalently bound to the protein surface, unless carbonate ligands are lost or replaced.

Crystallographic data indicate that the binding of these molecules does not alter the overall conformation of the protein, but it produces some changes around the dimetallic binding site. This work enlarges the repertoire of available structures of adducts formed upon the reaction of diruthenium compounds with proteins and provides new insights

into the reactivity of these compounds with biological macromolecules. Our results suggest that different diruthenium paddlewheel complexes can be used to prepare various artificial metalloenzymes with distinct properties. Data are significant because they support the idea that diruthenium complexes can be tuned, by changing the equatorial ligands, to direct their activity to specific cellular targets. Finally, our structures provide a very interesting system for molecular docking that can be used to predict metal compound binding sites on protein structures.

Conflicts of interest

Nothing to declare.

Acknowledgements

The authors thank Elettra staff for technical assistance. Comunidad de Madrid (Project S2017/BMD-3770-CM) and Universidad Complutense de Madrid (Program PR3/23) are gratefully acknowledged for the financial support. A. T. also acknowledges the Universidad Complutense for a Predoctoral Grant (CT63/19-CT64/19) and Research Stay Grant (EB25/22) and the Spanish Ministry of Science and Innovation for a Postgraduate Fellowship at Residencia de Estudiantes (2021–2022).

References

1 T. A. Stephenson and G. Wilkinson, New ruthenium carboxylate complexes, *J. Inorg. Nucl. Chem.*, 1966, **28**, 2285–2291.
2 M. J. Bennett, K. G. Caulton and F. A. Cotton, Structure of tetra-n-butyratodiruthenium chloride, a compound with a strong metal-metal bond, *Inorg. Chem.*, 1969, **8**, 1–6.
3 M. A. S. Aquino, Recent developments in the synthesis and properties of diruthenium tetracarboxylates, *Coord. Chem. Rev.*, 2004, **248**, 1025–1045.
4 P. Delgado-Martínez, L. Moreno-Martínez, R. González-Prieto, S. Herrero, J. L. Priego and R. Jiménez-Aparicio, Steric, Activation Method and Solvent Effects on the Structure of Paddlewheel Diruthenium Complexes, *Appl. Sci.*, 2022, **12**, 1000.
5 F. A. Cotton and A. Yokochi, Synthesis and Characterization of the Series of Compounds $Ru_2(O_2CMe)_x(admp)_{4-x}Cl$ (Hadmp = 2-Amino-4,6-dimethylpyridine, x = 3, 2, 1, 0), *Inorg. Chem.*, 1998, **37**, 2723–2728.
6 P. Angaridis, F. A. Cotton, C. A. Murillo, D. Villagrán and X. Wang, Paramagnetic Precursors for Supramolecular Assemblies: Selective Syntheses, Crystal Structures, and Electrochemical and Magnetic Properties of $Ru(O_2CMe)_{4-n}(formamidinate)_nCl$ Complexes, n = 1–4, *Inorg. Chem.*, 2004, **43**, 8290–8300.
7 P. Angaridis, in *Multiple Bonds Between Metal Atoms*, ed. F. A. Cotton, C. A. Murillo and R. A. Walton, Springer-Verlag, New York, 2005, pp. 377–430.
8 M. Cortijo, R. González-Prieto, S. Herrero, J. L. Priego and R. Jiménez-Aparicio, The use of amidinate ligands in paddlewheel diruthenium chemistry, *Coord. Chem. Rev.*, 2019, **400**, 213040.
9 W. R. Osterloh, G. Galindo, M. J. Yates, E. Van Caemelbecke and K. M. Kadish, Synthesis, Structural and Physicochemical Properties of Water-Soluble Mixed-Ligand Diruthenium Complexes Containing Anilinopyridinate Bridging Ligands, *Inorg. Chem.*, 2020, **59**, 584–594.
10 E. Van Caemelbecke, T. Phan, W. R. Osterloh and K. M. Kadish, Electrochemistry of metal-metal bonded diruthenium complexes, *Coord. Chem. Rev.*, 2021, **434**, 213706.
11 L. A. Miller-Clark, P. E. Christ and T. Ren, Diruthenium aryl compounds – tuning of electrochemical responses and solubility, *Dalton Trans.*, 2022, **51**, 580–586.
12 T. E. Vos, Y. Liao, W. W. Shum, J.-H. Her, P. W. Stephens, W. M. Reiff and J. S. Miller, Diruthenium Tetraacetate Monocation, $[Ru^{II/III}{}_2(O_2CMe)_4]^+$, Building Blocks for 3-D Molecule-Based Magnets, *J. Am. Chem. Soc.*, 2004, **126**, 11630–11639.
13 M. C. Barral, S. Herrero, R. Jiménez-Aparicio, M. R. Torres and F. A. Urbanos, A Spin-Admixed Ruthenium Complex, *Angew. Chem., Int. Ed.*, 2005, **44**, 305–307.
14 F. A. Cotton, S. Herrero, R. Jiménez-Aparicio, C. A. Murillo, F. A. Urbanos, D. Villagrán and X. Wang, How Small Variations in Crystal Interactions Affect Macroscopic Properties, *J. Am. Chem. Soc.*, 2007, **129**, 12666–12667.
15 M. C. Barral, D. Casanova, S. Herrero, R. Jiménez-Aparicio, M. R. Torres and F. A. Urbanos, Tuning the Magnetic Moment of $[Ru_2(DPhF)_3(O_2CMe)L]^+$ Complexes (DPhF=N,N′-Diphenylformamidinate): A Theoretical Explanation of the Axial Ligand Influence, *Chem. – Eur. J.*, 2010, **16**, 6203–6211.
16 G. M. Chiarella, F. A. Cotton, C. A. Murillo, K. Ventura, D. Villagrán and X. Wang, Manipulating Magnetism: Ru_2^{5+} Paddlewheels Devoid of Axial Interactions, *J. Am. Chem. Soc.*, 2014, **136**, 9580–9589.
17 D. de Oliveira Silva, Perspectives for Novel Mixed Diruthenium-Organic Drugs as Metallopharmaceuticals in Cancer Therapy, *Anti-Cancer Agents Med. Chem.*, 2010, **10**, 312–323.
18 G. Ribeiro, M. Benadiba, D. de Oliveira Silva and A. Colquhoun, The novel ruthenium—γ-linolenic complex $[Ru_2(aGLA)_4Cl]$ inhibits C6 rat glioma cell proliferation and induces changes in mitochondrial membrane potential, increased reactive oxygen species generation and apoptosis in vitro, *Cell Biochem. Funct.*, 2010, **28**, 15–23.
19 M. Benadiba, I. de M. Costa, R. L. S. R. Santos, F. O. Serachi, D. de Oliveira Silva and A. Colquhoun, Growth inhibitory effects of the Diruthenium-Ibuprofen compound, $[Ru_2Cl(Ibp)_4]$, in human glioma cells in vitro and in the rat C6 orthotopic glioma in vivo, *J. Biol. Inorg. Chem.*, 2014, **19**, 1025–1035.

20 J. A. Miyake, M. Benadiba, G. Ribeiro, D. de Oliveira Silva and A. Colquhoun, Novel Ruthenium – Gamma-linolenic Acid Complex Inhibits C6 Rat Glioma Cell Proliferation In Vitro and in the Orthotopic C6 Model In Vivo After Osmotic Pump Infusion, *Anticancer Res.*, 2014, **34**, 1901.

21 H. U. Rehman, T. E. Freitas, R. N. Gomes, A. Colquhoun and D. de Oliveira Silva, Axially-modified paddlewheel diruthenium(II,III)-ibuprofenato metallodrugs and the influence of the structural modification on U87MG and A172 human glioma cell proliferation, apoptosis, mitosis and migration, *J. Inorg. Biochem.*, 2016, **165**, 181–191.

22 S. R. Alves Rico, A. Z. Abbasi, G. Ribeiro, T. Ahmed, X. Y. Wu and D. de Oliveira Silva, Diruthenium(II,III) metallodrugs of ibuprofen and naproxen encapsulated in intravenously injectable polymer–lipid nanoparticles exhibit enhanced activity against breast and prostate cancer cells, *Nanoscale*, 2017, **9**, 10701–10714.

23 S. R. Alves, A. Colquhoun, X. Y. Wu and D. de Oliveira Silva, Synthesis of terpolymer-lipid encapsulated diruthenium(II,III)-anti-inflammatory metallodrug nanoparticles to enhance activity against glioblastoma cancer cells, *J. Inorg. Biochem.*, 2020, **205**, 110984.

24 I. Coloma, M. Cortijo, I. Fernández-Sánchez, J. Perles, J. L. Priego, C. Gutiérrez, R. Jiménez-Aparicio, B. Desvoyes and S. Herrero, pH- and Time-Dependent Release of Phytohormones from Diruthenium Complexes., *Inorg. Chem.*, 2020, **59**, 7779–7788.

25 E. Barresi, I. Tolbatov, T. Marzo, E. Zappelli, A. Marrone, N. Re, A. Pratesi, C. Martini, S. Taliani, F. Da Settimo and D. La Mendola, Two mixed valence diruthenium(II,III) isomeric complexes show different anticancer properties, *Dalton Trans.*, 2021, **50**, 9643–9647.

26 L. Messori, T. Marzo, R. N. F. Sanches, H. U. Rehman, D. de Oliveira Silva and A. Merlino, Unusual Structural Features in the Lysozyme Derivative of the Tetrakis(acetato) chloridodiruthenium(II,III) Complex, *Angew. Chem., Int. Ed.*, 2014, **53**, 6172–6175.

27 F. Lupi, T. Marzo, G. D'Adamio, S. Cretella, F. Cardona, L. Messori and A. Goti, Diruthenium Diacetate Catalysed Aerobic Oxidation of Hydroxylamines and Improved Chemoselectivity by Immobilisation to Lysozyme, *ChemCatChem*, 2017, **9**, 4225–4230.

28 A. Terán, G. Ferraro, A. E. Sánchez-Peláez, S. Herrero and A. Merlino, Effect of equatorial ligand substitution on the reactivity with proteins of paddlewheel diruthenium complexes: structural studies, *Inorg. Chem.*, 2023, **62**, 670–674.

29 I. Tolbatov and A. Marrone, Kinetics of Reactions of Dirhodium and Diruthenium Paddlewheel Tetraacetate Complexes with Nucleophilic Protein Sites: Computational Insights, *Inorg. Chem.*, 2022, **61**, 16421–16429.

30 A. Bino, F. A. Cotton and T. R. Felthouse, Structural studies of some multiply bonded diruthenium tetracarboxylate compounds, *Inorg. Chem.*, 1979, **18**, 2599–2604.

31 M. C. Barral, R. González-Prieto, S. Herrero, R. Jiménez-Aparicio, J. L. Priego, M. R. Torres and F. A. Urbanos, Anionic dihalotetraacetatodiruthenium(II,III) compounds, *Polyhedron*, 2005, **24**, 239–247.

32 Y. Hiraoka, T. Ikeue, H. Sakiyama, F. Guégan, D. Luneau, B. Gillon, I. Hiromitsu, D. Yoshioka, M. Mikuriya, Y. Kataoka and M. Handa, An unprecedented up-field shift in the ^{13}C NMR spectrum of the carboxyl carbons of the lantern-type dinuclear complex TBA$[Ru_2(O_2CCH_3)_4Cl_2]$ (TBA^+ = tetra(n-butyl)ammonium cation), *Dalton Trans.*, 2015, **44**, 13439–13443.

33 K. Uemura, N. Uesugi, A. Matsuyama, M. Ebihara, H. Yoshikawa and K. Awaga, Integration of Paramagnetic Diruthenium Complexes into an Extended Chain by Heterometallic Metal–Metal Bonds with Diplatinum Complexes, *Inorg. Chem.*, 2016, **55**, 7003–7011.

34 T. Miyazawa, T. Suzuki, Y. Kumagai, K. Takizawa, T. Kikuchi, S. Kato, A. Onoda, T. Hayashi, Y. Kamei, F. Kamiyama, M. Anada, M. Kojima, T. Yoshino and S. Matsunaga, Chiral paddle-wheel diruthenium complexes for asymmetric catalysis, *Nat. Catal.*, 2020, **3**, 851–858.

35 B. S. Kennon, J.-H. Her, P. W. Stephens, W. W. Shum and J. S. Miller, Structure and Magnetic Ordering of $K_xH_{1-x}Ni(OH_2)_4[Ru_2(CO_3)_4]\cdot zH_2O$, *Inorg. Chem.*, 2007, **46**, 9033–9035.

36 B. S. Kennon, J.-H. Her, P. W. Stephens and J. S. Miller, Diruthenium Tetracarbonate Trianion, $[Ru^{II/III}{}_2(O_2CO)_4]^{3-}$, Based Molecule-Based Magnets: Three-Dimensional Network Structure and Two-Dimensional Magnetic Ordering, *Inorg. Chem.*, 2009, **48**, 6117–6123.

37 B. Liu, Y.-Y. Jia, J. Jin, X.-M. Liu, D. Wang and G.-L. Xue, Cadmium diruthenium(II,III) carbonates showing diverse magnetism behavior arising from variety configuration of $[Ru_2(CO_3)_4]_n{}^{3n-}$ layer, *Dalton Trans.*, 2013, **42**, 10208.

38 B. Liu, Y.-Y. Jia, J. Jin, X.-M. Liu and G.-L. Xue, Layer structural bimetallic metamagnets obtained from the aggregation of $Ru_2(CO_3)_4{}^{3-}$ and Co^{2+} in existence of halogen, *CrystEngComm*, 2013, **15**, 4280.

39 G.-H. Wu, J. Jin, Y.-Y. Jia, J.-H. Yang and B. Liu, Axial ligands of Ru_2 tuning Zn^{2+} rearrangement to form a new heterometallic carbonate: Synthesis, structure and magnetic properties, *Inorg. Chem. Commun.*, 2014, **50**, 58–61.

40 J.-H. Yang, R.-M. Cheng, Y.-Y. Jia, J. Jin, B.-B. Yang, Z. Cao and B. Liu, Chlorine and temperature directed self-assembly of Mg–Ru_2(II,III) carbonates and particle size dependent magnetic properties, *Dalton Trans.*, 2016, **45**, 2945–2954.

41 P. Delgado-Martínez, R. González-Prieto, S. Herrero, R. Jiménez-Aparicio, J. Perles, J. L. Priego, M. R. Torres and B. Sufrate, Preparation of Crystalline Phases of 3D Coordination Polymers Based on Tetracarbonatodiruthenium Units and Lanthanide(III) Ions – Magnetic Characterization, *Eur. J. Inorg. Chem.*, 2017, **2017**, 3161–3168.

42 D. Gutiérrez-Martín, M. Cortijo, Á. Martín-Humanes, R. González-Prieto, P. Delgado-Martínez, S. Herrero, J. Priego and R. Jiménez-Aparicio, Tetracarbonatodiruthenium Fragments and Lanthanide(III) Ions as Building Blocks to Construct 2D Coordination Polymers, *Polymers*, 2019, **11**, 426.

43 J.-Y. Li, Y.-C. Tian, L.-N. Feng, Z.-Q. Zhou, L.-L. Wang, J.-H. Yang and B. Liu, Enhancing magnetic hardness by sonication assisted synthesis of heterometallic carbonato spin-glass $Na[Ni(H_2O)_4Ru_2(CO_3)_4]\cdot 3H_2O$, *Chem. Commun.*, 2020, **56**, 1369–1372.

44 F. A. Cotton, L. Labella and M. Shang, Further study of tetracarbonato diruthenium(II,III) compounds, *Inorg. Chem.*, 1992, **31**, 2385–2389.

45 A. Terán, M. Cortijo, Á. Gutiérrez, A. E. Sánchez-Peláez, S. Herrero and R. Jiménez-Aparicio, Ultrasound-assisted synthesis of water-soluble monosubstituted diruthenium compounds, *Ultrason. Sonochem.*, 2021, **80**, 105828.

46 K. Nakamoto, in *Infrared and Raman Spectra of Inorganic and Coordination Compounds*, John Wiley & Sons, Ltd, Hoboken, New Jersey, 2009, vol. Part B, pp. 1–273.

47 A. Inchausti, A. Terán, A. Manchado-Parra, A. de Marcos-Galán, J. Perles, M. Cortijo, R. González-Prieto, S. Herrero and R. Jiménez-Aparicio, New insights into progressive ligand replacement from $[Ru_2Cl(O_2CCH_3)_4]$: synthetic strategies and variation in redox potentials and paramagnetic shifts, *Dalton Trans.*, 2022, **51**, 9708–9719.

48 I. Coloma, M. Cortijo, M. J. Mancheño, M. E. León-González, C. Gutierrez, B. Desvoyes and S. Herrero, Diruthenium complexes as pH-responsive delivery systems: a quantitative assessment, *Inorg. Chem. Front.*, 2023, DOI: **10.1039/D3QI00399J**.

49 K. Sikora, M. Jaśkiewicz, D. Neubauer, D. Migoń and W. Kamysz, The Role of Counter-Ions in Peptides—An Overview, *Pharmaceuticals*, 2020, **13**, 442.

50 S. Das, P. Ghosh, S. Koley and A. S. Roy, Binding of naringin and naringenin with hen egg white lysozyme: A spectroscopic investigation and molecular docking study, *Spectrochim. Acta, Part A*, 2018, **192**, 211–221.

51 Z. Wang, D. Li and J. Jin, Study on the interaction of puerarin with lysozyme by spectroscopic methods, *Spectrochim. Acta, Part A*, 2008, **70**, 866–870.

52 M. C. Vaney, S. Maignan, M. Riès-Kautt and A. Ducruix, High-Resolution Structure (1.33 Å) of a HEW Lysozyme Tetragonal Crystal Grown in the APCF Apparatus. Data and Structural Comparison with a Crystal Grown under Microgravity from SpaceHab-01 Mission, *Acta Crystallogr., Sect. D: Biol. Crystallogr.*, 1996, **52**, 505–517.